Steel and Composite Structures, *Vol. 24, No. 2 (2017) 177-189*
DOI: https://doi.org/10.12989/scs.2017.24.2.177

Mechanical behavior of stud shear connectors embedded in HFRC

Yu-Liang He [1,2], Xu-Dong Wu [1], Yi-Qiang Xiang [*2,3], Yu-Hang Wang [2], Li-Si Liu [2] and Zhi-Hai He [1]

[1] *College of Civil Engineering, Shaoxing University, Shaoxing 312000, China*
[2] *College of Civil Engineering and Architecture, Zhejiang University, Hangzhou 310058, China*
[3] *Cyrus Tang Center for Sensor Materials and Applications, Hangzhou 310058, China*

(*Received October 15, 2016, Revised March 08, 2017, Accepted March 20, 2017*)

Abstract. Hybrid-fiber reinforced concrete (HFRC) may provide much higher tensile and flexural strengths, tensile ductility, and flexural toughness than normal concrete (NC). HFRC slab has outstanding advantages for use as a composite bridge potential deck slab owing to higher tensile strength, ductility and crack resistance. However, there is little information on shear connector associated with HFRC slabs. To investigate the mechanical behavior of the stud shear connectors embedded in HFRC slab, 14 push-out tests (five batches) in HFRC and NC were conducted. It was found that the stud shear connector embedded in HFRC had a better ductility, higher stiffness and a slightly larger shear bearing capacity than those in NC. The experimentally obtained ultimate resistances of the stud shear connectors were also compared against the equations provided by GB50017 2003, ACI 318-112011, AISC 2011, AASHTO LRFD 2010, PCI 2004, and EN 1994-1-1 (2004), and an empirical equation to predict the ultimate shear connector resistance considering the effect of the HFRC slabs was proposed and validated by the experimental data. Curve fitting was performed to find fitting parameters for all tested specimens and idealized load-slip models were obtained for the specimens with HFRC slabs.

Keywords: headed stud; push-out test; HFRC; shear bearing capacity; load-slip

1. Introduction

In recent years, fiber-reinforced concrete (FRC) is well known for its enhanced tensile and flexural strengths, tensile ductility, and flexural toughness (ACI 2009). The inherent properties of conventional concrete can be dramatically improved by addition of fiber with a relatively low volume (typically ≤ 2%) owing to the crack arrest mechanism. These properties make FRC attractive for the use in structural applications. At present, steel fiber (SF) and polypropylene fiber (PF) are most widely applied in civil engineering. However, it is also recognized that the strength and ductility of concrete is partially improved by inclusion of only single SF or single PF, and PF are found to improve the tensile strain capacity of FRC whereas SF contributed on the improvement of ultimate tensile strength of FRC. Prisco *et al.* (2009) Combined different types of fibers to optimize the mechanical performance of concrete, which resulted in HFRC materials.

Substantial experimental studies on HFRC have been conducted. For example, Caggiano *et al.* (2016) presented the mechanical properties of HFRC in terms of the results of experimental tests under compression and in bending. Chi (2012) and Chi *et al.* (2014a, b) studied the mechanical behavior of HFRC under uniaxial compression through orthogonal experimental method and set up the plasticity theory based constitutive modeling of HFRC. Kim *et al.* (2016) used SF and PF to control and mitigate cracks in concrete, and the physical properties as crack resistance capabilities of the HFRC were evaluated. Demir (2015) developed an artificial neural network (ANN) model to predict the compressive and bending strengths of HFRC. Comparisons between the ANN analysis and the experimental results were performed and a fairly good agreement was found. Tuan *et al.* (2014) investigated that the effects of PF, SF and hybrid on the properties of high strength fiber reinforced self-consolidating concrete (HSFR-SCC) under different volume contents. It was found that splitting tensile and flexural strengths of concrete were mainly improved by SF, whereas the inclusion of PF resulted in the better efficiency in the improvement of toughness. It also was showed that HSFR-SCC had enough endurance against deterioration, lower chloride ion penetrability and reinforcement corrosion rate.

Steel-concrete composite structures utilizing the advantages of both steel and concrete are widespread in structural engineering, which offers the advantages of construction efficiency, durability and improved economy. But increasing vehicle traffic and increasing axle loads have significantly increased the number and amplitude of loading cycles experienced on a daily basis by composite bridges, at the same time existing composite bridges are suffering from aging and deterioration due to harsh environmental exposure conditions and/or are damaged by natural (earth-quakes, hydrologic forces, etc.). When it comes to the most common problems associated with existing composite bridges, the results of those survey indicate that the deterioration of concrete decks is one of the most pronounced problems in existing composite (steel-concrete) bridges. In this respect, a potential solution which has been

*Corresponding author, Ph.D., Professor,
E-mail: Xiangyiq@zju.edu.cn

http://www.techno-press.org/?journal=scs&subpage=6
ISSN: 1229-9367 (Print), 1598-6233 (Online)

developed during the past decades is the application of fiber reinforced polymer (FRP) composite bridge decks, but their fairly high initial cost prevents the widespread application of these decks (Mara *et al*. 2014). It also needs good solutions to solve the connection of the FRP slab and steel beam. However, the HFRC decks have outstanding advantages in crack resistance, tensile ductility, flexural toughness and high tensile strength. The cost is no higher than the conventional concrete decks, and reduces greatly in comparison with FRP. This paper aims to introduce HFRC slab into steel-concrete composite bridge in place of conventional concrete slab.

The association of steel beams and HFRC decks as a constructive solution has not been thoroughly researched. Few studies have been conducted to understand the connection between these elements, but this understanding is of great importance for enabling a better use of this system. In composite beams, the mechanical action provided by the shear connector guarantees the transfer of shear forces at the interface between the steel beam and the decks. Among these connectors, headed studs are the most commonly used due to their flexible behaviour, which allows a high longitudinal slip between the concrete and steel before the ultimate limit state is reached. Up to now, the resistance and load–slip behavior of stud shear connections have been experimentally and numerically evaluated by various researchers. Lam and El-Lobody (2005) proposed a numerical model using the finite element method to simulate the push-out tests. The effectiveness of the model was proved by comparing the numerical outputs with the test results and data given in the current design codes. Xue *et al*. (2012) carried out 12 push-out tests to investigate the behavior of different stud connections with single-stud or multi-stud connectors, and a new expression for the stud load-slip relationship was proposed. Nguyen *et al*. (2014) presented an experimental investiga-tion on the shear connections between carbon/glass Fiber-Reinforced Polymer I-girder and Ultra-High Performance Fiber-Reinforced Concrete slabs through fourteen push-out tests to evaluate the load–slip behavior and the ultimate resistance of the bolt shear connectors. An and Cederwall (1996) presented results from push out tests of studs embedded in normal and high strength concrete. They found that the concrete compressive strength significantly affected the strength of the stud connections. They suggested a design formula to estimate the shear strength of studs embedded in high strength concrete considering the interaction between the studs and the surrounding concrete. Han *et al*. (2015) conducted Push-out tests to investigate the static behavior of steel and rubber-filled concrete composite beams with different rubber mixed concrete and studs. Kim *et al*. (2015) investigated stud shear connectors embedded in an ultrahigh-performance concrete (UHPC) deck through 15 push-out tests, and showed that the stud shear connectors in a UHPC deck should be designed according to the elastic criterion. Although extensive studies were carried out for shear connections of steel-concrete composite beam systems, however it provides only marginal insights into shear connections of steel-HFRC composite beam system. The main difference between the steel–conventional concrete and the steel-HFRC beam systems is the environment surrounding the stud shear connectors. In the steel–conventional concrete composite beam system, headed studs are embedded in the NC deck. On the other hand, shear connectors embed in the HFRC deck in the steel-HFRC system. As a result, the load–slip behavior of the shear connections for the steel-conventional concrete beam system may be different from that for the steel–HFRC beam system. In addition, previous studies mainly focused on behavior of studs embedded in lightweight, normal weight, normal strength concrete and high-strength concrete. The use of HFRC may result in significant improvement of the properties of stud connections.

This paper is to firstly contribute to the study of the association between steel beams and HFRC decks by affecting the performance of the stud shear connectors. The parameters considered in this study are the number of studs, deck types and the spacing of studs. Secondly, because equations to predict the load–slip behavior and the ultimate resistance of shear connectors embedded in the HFRC are not available up to now. This study aims in evaluating the load–slip behavior and the ultimate shear connector resistance of shear connectors embedded in the HFRC decks through push-out tests, and proposed empirical equations.

2. Design and fabrication of the push-out test specimens

2.1 Preparations of test specimens

14 push-out test specimens were designed in accordance with EN 1994-1-1 (2004), which were divided into 5 batches. For simplicity, the HFRC specimens were abbreviated as HFTC (HFTC-III to HFTC-III), while the NC specimens, as NTC (NTC-I to NTC-II). Table 1 listed the design parameters of push-out specimens. Three specimens A, B and C were prepared for NTC-I, NTC-II, HFTC-III and HFTC-II, while HFTC-III only prepare two specimens A and B. The variables of the test program were the number of studs, deck types, the stud diameter and spacing of studs. The NTC cases were specimens with conventional reinforced concrete slabs for the purpose of comparison.

The HFTC-III and HFTC-II cases had identical dimensions to the NTC-I and NTC-II cases respectively and differed only that the slab was made of HFTC instead of NC. Both the NTC-I and the HFTC-III specimens had the same dimensions, while the NTC-II and the HFTC-II specimens had the same dimensions. Xue *et al*. (2012) showed that the number of stud effect on static behavior of shear connector is negligible, and the study only provided shear connectors in one layer. Studs with two different diameters were used: 22 mm for NTC-I and HFTC-III and 16mm for the other batches, as shown in Table 1. The stud diameters were chosen according to the thickness of the deck to meet the requirement of aspect ratio of four and the lengths given for the studs are as-welded lengths. The steel beam of the specimens using H-profile steel welded with

Table 1 Parameters of push-out test specimens

Specimen		Slab thickness /(mm)	Stud number	Distribution of the stud	Space of stud /(mm)	Specification of stud /(mm × mm)
NTC-I	A	150	1×2	horizontal	—	Φ22×100
	B	150	2×2	horizontal	100	Φ22×100
	C	150	3×2	horizontal	100	Φ22×100
HFTC-III	A	150	1×2	horizontal	—	Φ22×100
	B	150	2×2	horizontal	100	Φ22×100
	C	150	3×2	horizontal	100	Φ22×100
NTC-II	A	150	2×2	horizontal	50	Φ16×80
	B	150	2×2	horizontal	100	Φ16×80
	C	150	2×2	horizontal	150	Φ16×80
HFTC-II	A	150	2×2	horizontal	50	Φ16×80
	B	150	2×2	horizontal	100	Φ16×80
	C	150	2×2	horizontal	150	Φ16×80
HFTC-III	A	150	2×2	verticality	180	Φ16×80
	B	150	2×2	verticality	90	Φ16×80

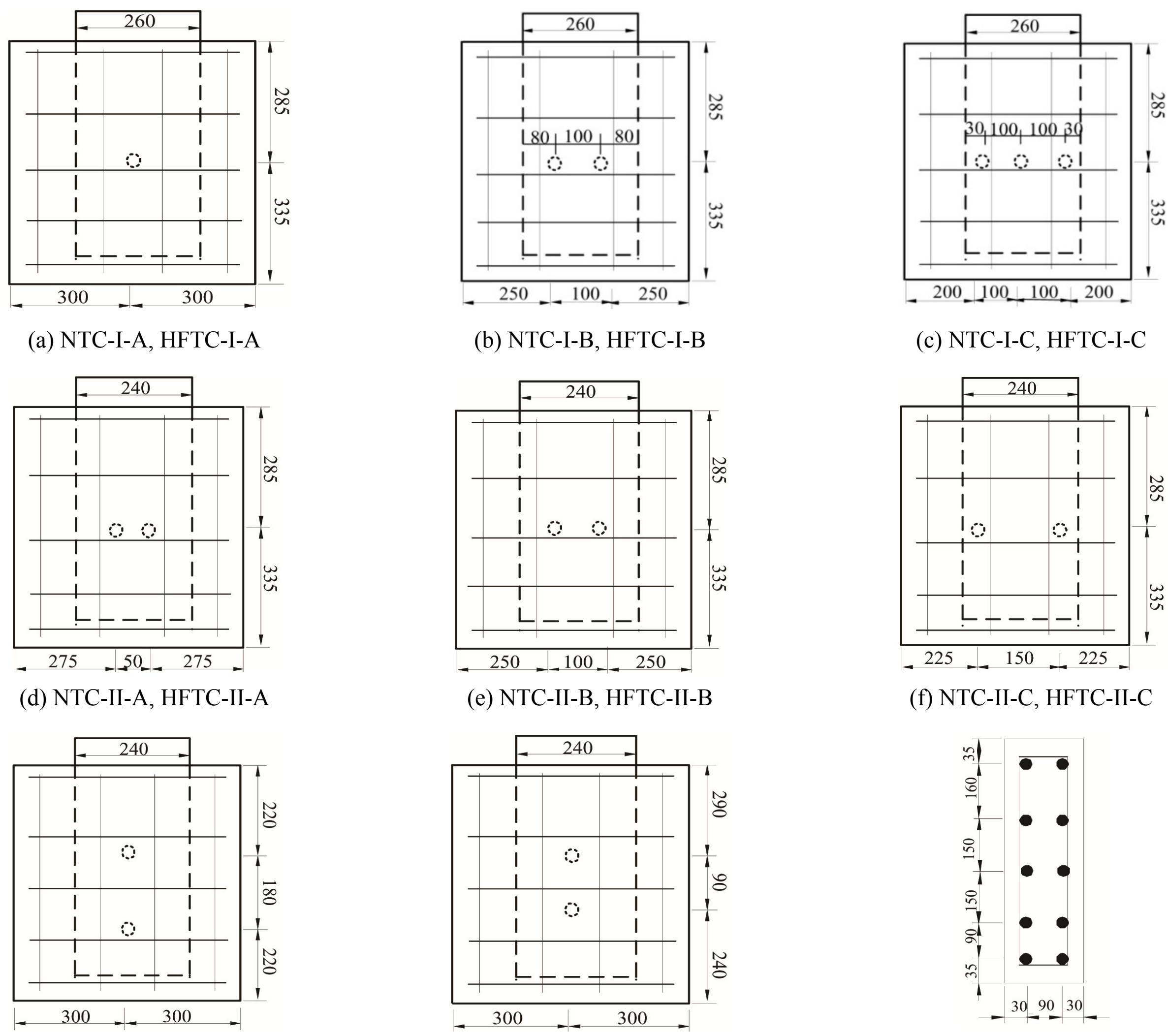

(a) NTC-I-A, HFTC-I-A (b) NTC-I-B, HFTC-I-B (c) NTC-I-C, HFTC-I-C

(d) NTC-II-A, HFTC-II-A (e) NTC-II-B, HFTC-II-B (f) NTC-II-C, HFTC-II-C

(g) HFTC-III-A (h) HFTC-III-B (i) Distribution of bar

Fig. 1 Specimens geometry of push-out tests steel plate. The studs were automatically welded to each flange of the steel beam by electro fusion. The steel beam section was 260×260×16×16 for NTC-I and HFTC-III, and 240×240×12×12 for NTC-II, HFTC-II and HFTC-III. Two layers steel bars (Φ12 mm) were placed in the concrete slab, and spacing of longitudinal and transverse directions as shown in Fig. 1. Fig. 1 also shows the dimensions of all specimens.

Generally, the concrete grade of the slab decks varies from 40 to 50 Mpa (28-days 150 mm cubic compressive strength) in bridge engineering in china, and so the concrete slabs used in the push-out tests were made of concrete with cube compressive strength of approximately 50 Mpa in this paper. Qian and Stroeven (2000) showed that a certain content of fine particles such as fly ash was necessary to evenly disperse fibers, and the fly ash particles were added into the concrete mixture. According to CECS (2004), to take full of the advantage in strength improvement and toughness, the volume fraction of SF is suggested between 0.5 and 2.0% and the aspect ratio is suggested between 30 and 80. Hence, corrugated SF with tensile strength over 600 MPa are used at volume fraction of 1%, and aspect ratio (length/diameter) of 30 are employed in this study. According to the product instruction of PF, a low volume fraction from 0.05 to 0.2% is suggested considering the homogeneity to ensure the evenly distribution of PF. Hence, PF with an elongation rate between 15 and 35% is used at volume fraction of 0.15% with a diameter of 0.048 mm, and the length of the fiber is selected as 8 mm in the study. Table 2 lists the mixture proportion of HFRC and NC. Each specimen was cast in the vertical position, and bonding and friction at the interface between the flanges of the steel beam and the concrete slab were prevented by greasing the flanges. The prisms and cubes specimens were cast at the same time as the push-out test specimens. These concrete specimens were cured in standard laboratory conditions, which submerged in water according to the concrete standard.

2.2 Material properties

The 28-day compressive strength of concrete was obtained from the 150 mm cube uniaxial compressive tests. A standard prism (150 mm × 150 mm × 300 mm) was used to determine the 28-daymodulus of elasticity of the concrete. The uniaxial tensile strength of concrete was tested by prism specimens (150 mm × 150 mm × 460 mm). The concrete cylinder compressive strength was obtained through the conversion of the cubic compressive strength, while the secant elastic modulus of concrete was obtained through the conversion of the 28-day modulus of elasticity. Table 3 presented the average values of compressive and tensile strength and the modulus of elasticity. The modulus of elasticity of the steel and stud is 206 GPa. The mechanical properties of the fibers, headed studs, reinforcing bars and steel plate were provided by the manufacturer. Table 4 lists the properties of the reinforcing bars, steel plates, and studs. Table 5 lists the physical characteristics of the SF and PF.

Chi *et al*. (2014b) developed an equation for calculating the HFRC uniaxial compressive strength on the basis of the test results as well as the variance analyses.

$$f_{fc} = f_c(1 + 0.206\lambda_{sf} + 0.388\lambda_{pf}) \tag{1}$$

Huang (2004) suggested PF's impact on the elastic stiffness of HFRC can be regarded as negligible, and it is therefore assumed that the value of elastic modulus has the

Table 2 Mixture proportion of HFRC and NC

Concrete	Water	Cement	Fly ash particle	Sand	Gravel	Steel	Polypropylene
HFRC	190	486	108	571	945	1% (23 kg/m³)	0.15% (3.45 kg/m³)
NC	190	486	108	571	945	0	0

Table 3 28-daycompressive and tensile strength and modulus of elasticity of concrete

Specimen	Compression strength /MPa	Elastic modulus /MPa	Tensile strength /MPa
NC	49.2 (38.9) [a]	33.98 (29.06) [b]	3.49
HFRC	57.1 (45.1) [a]	35.4 (30.27) [b]	4.48

[a] the concrete cylinder compressive strength; [b] the secant elastic modulus of concrete

Table 4 Properties of reinforcement, steel plate and stud

Component	Specification(mm)	Elongation rate (%)	Tensile strength f_u (MPa)	Yield strength f_y (MPa)
Stud	Φ16	16	450	385
Stud	Φ22	17	430	365
Steel plate	12	26.5	585	460
Steel plate	16	27	540	435

[a] the concrete cylinder compressive strength; [b] the secant elastic modulus of concrete

Table 5 Properties of SF and PF

Fibers	Length (mm)	Average diameter (mm)	Length/ diameter	Tensile strength (MPa)	Young's modulus (Gpa)	Density (kg/m^3)
SF	28	0.7	40	600	210	7800
PF	8	0.048	167	296	—	910

following relationship with the SF volume fraction.

$$E_{fc} = \frac{10^5}{2.2 + 34.74 / f_{fc}} \tag{2a}$$

$$f_{fc} = f_c (1 + 0.056\lambda_{sf}) \tag{2b}$$

Zhang (2010) fitted an equation for calculating the HFRC uniaxial tensile strength according to the experimental results.

$$f_{ft} = f_t (1 + 0.379\lambda_{sf} + 0.244\lambda_{pf}) \tag{3}$$

where f_{fc} , f_c are the cube compression strength of HFRC and NC (MPa), respectively; f_{ft}, f_t are the tensile strength of HFRC and NC (MPa), respectively; E_{fc} is the elastic modulus of HFRC (Pa); λ_{sf} is the SF reinforcement index calculated as $\lambda_{sf} = V_{sf}(l_{sf}/d_{sf})$; V_{sf} is the volume fraction of SF; l_{sf}/d_{sf} is the aspect ratio of SF; λ_{pf} is the PF reinforcements index calculated as $\lambda_{pf} = V_{pf}(l_{pf}/d_{pf})$; V_{pf} is the volume fraction of PF; and l_{pf}/d_{pf} is the aspect ratio of PF.

Applying Eqs. (1)-(3) to calculate the uniaxial compressive and tensile strength and the elastic modulus of HFRC are 58.03 Mpa, 35.78 Mpa and 4.23 Mpa respectively, and the test results are 57.1 Mpa, 35.4 Mpa and 4.48 Mpa as listed in Table 3. It is said that the experimental results of HFRC agree well with the calculated results.

2.3 Loading procedure and measurement of the push-out test

The test setup used in the experiments is shown in Fig. 2. The steel support was very smooth and some minor sand was only used between the concrete of the pot and the support. The specimens were tested using a servo hydraulic testing machine with a capacity of 4000 kN. The procedure of testing was carried out in accordance with EN 1994-1-1 (2004). The load was applied in increments of 5 kN from 0 to 40% of the expected failure loads (EFL) estimated from EN 1994-1-1 (2004), then returned to 5% of the EFL, and then the loading cycle between 5% and 40% of the EFL was repeated 25 times to eliminate the effect of the chemical adhesion between the concrete slab and steel beam during the test. After that, the slip controlled load continued up to the failure at the speed of 1 mm/1 min of slip up to the failure. The relative slip between each concrete slab and the steel section of the push-out specimens was measured continuously during loading by using two 1/1000 mm LVDTs (Linear Variable Differential Transformer).

Fig. 2 Loading of push out test specimen

3. Results of the push-out test

3.1 Failure mode

The pattern of failure observed from all the specimens was the stud shank failure, and the breakout failure of concrete slabs was not observed for all the tested specimens owing to the concrete strength being higher. Due to the manufacturing process of the specimen the two sides of the specimens normally did not have the same resistance. This may be also attributed to the manufacturing imperfections of the shear connectors, preventing them to attain their full shear resistance on each side of the specimens. The studs always yielded first on one side of the specimen in the loading process, and then the specimen was broken. There was accentuated curvature at the base of the stud connector on the side broken firstly (Fig. 3). Fig. 3 shows the typical failure pattern of stud and concrete plate. Table 6 lists shear capacity and slippage of all specimens. The push-out tests conducted on HFTC-III aimed to determine the influence of the stud number on the properties of the stud connectors. The single stud of the shear bearing capacity was biggest for the specimen HFTC-I-B (Table 6). The middle stud experienced the greatest plastic deformation for the specimen HFTC-I-C among three headed studs (Fig. 3). The cracks distribution ranges of the HFRC slabs became larger around the studs with increasing stud numbers. The push-out tests conducted on HFTC-II aimed to investigate the influence of the stud transverse space on the properties of the stud connectors. When the stud's spacing narrowed, the shear deformation of the studs increased (Fig. 3 and Table 6). The cracks of the concrete slab between the studs increased with the stud's spacing narrowed. The push-out tests conducted on HFTC-III aimed to determine the influence of the stud vertical space on the properties of the stud connectors. The upper headed studs had a greater plastic deformation than the lower headed studs for the specimens HFTC-III, as shown in Fig. 3. The concrete's

Fig. 3 Failure of push-out test specimens

Table 6 Shear capacity and slip of specimens

Specimen	NTC-I			HFTC-I			NTC-II			HFTC-II			HFTC-III	
	A	B	C	A	B	C	A	B	C	A	B	C	A	B
P_u	152.5	162.5	155.5	157.5	169.6	157.2	78.8	78.8	73.8	82.5	81.3	82.5	73.8	78.8
S_{max}	7.08	8.45	11	7.13	9.43	14.42	6.31	4.44	3.61	6.5	4.66	3.84	5.98	6.22
S_u	8.51	8.95	12.06	9	9.69	15.5	6.71	4.79	4.37	7.26	5.22	5.09	6.64	7.12

* P_u ultimate shear bearing capacity per stud (kN)
S_{max} slippage of maximum shear capacity (mm),
S_u slippage of failure (mm)

local crushing below the upper studs was more severe for specimens HFTC-III. The NTC-I and NTC-II cases were specimens with conventional reinforce concrete slab for the purpose of comparison. The local concrete was crushed below the studs for NTC specimens, and the cracks occurred only below the studs in a radial direction.

Compared with the NTC slabs, HFTC concrete slabs were also crushed locally below the studs when the specimens were broken, and the degree of damage was slighter, which might be attributed to the high compressive strength, high ductility, and high crack resistance of the HFRC slabs after SF and PF incorporated into concrete. The multiple cracks surrounding bearing regions of the shear connectors inside the HFTC slabs were found. The cracks were longer, and distributed wider, but the crack's width was smaller than that of the NC slabs, possibly because of the process of distributed micro-cracking in the HFRC slabs and the bridging effects of SF and PF.

3.2 The load-slip curve and stiffness of the headed stud connector

When all specimens bore an external load, the slip between the concrete slab and H-profile steel occurred. Fig. 4 shows the load-slip curve of the HFTC specimens for different parameters. The load-slip curve of the HFTC specimens could be divided into three different phases. The first phase was the elastic stage (ES), which showed an almost linear initial progression. At the ES, the slip was very small for all of the specimens, and the stud connector showed large shear stiffness in the ES. The HFTC-I specimens lie in the ES when the load is less than approximately 60% of the maximum load value, and approximately 65% for HFTC-II and HFTC-III specimens. The curves developed a new trend with a softer slope when the load exceeds the elastic value. The load-slip curves started to enter the flow-plastic stage (FPS). The slip increased rapidly when the load increased slowly, and the stud shear stiffness decreased continuously. The specimens enter into descent stage (DS) when the load attained the maximum load value, and the specimens began to yield and failed. Fig. 5 shows the comparison of the load-slip curves between the NTC and HFTC specimens. In comparison with NTC specimens, the FPS and DS of the HFRC specimens were little longer, and the cause may be that the fibers in the HFTC slabs prevented the concrete cracks from

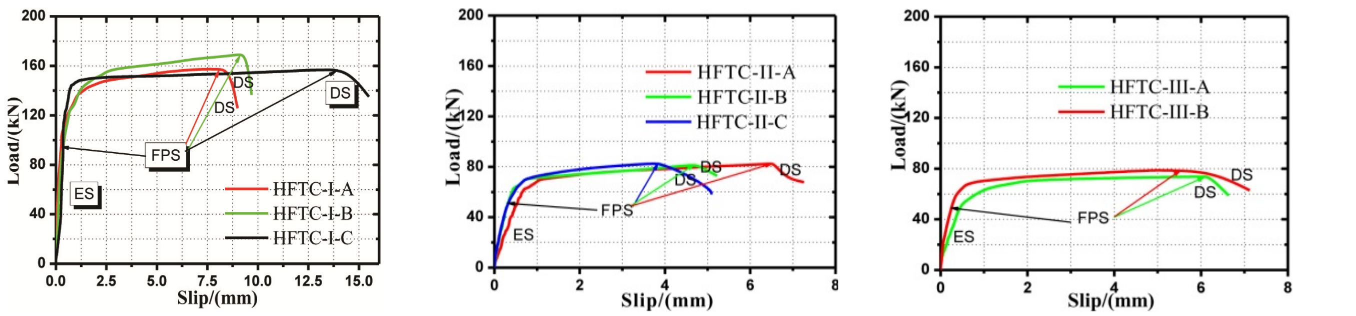

(a) HFTC-I specimens (b) HFTC-II specimens (c) HFTC-III specimens

Fig. 4 Load-slip curve of different parameters for HFTC specimens

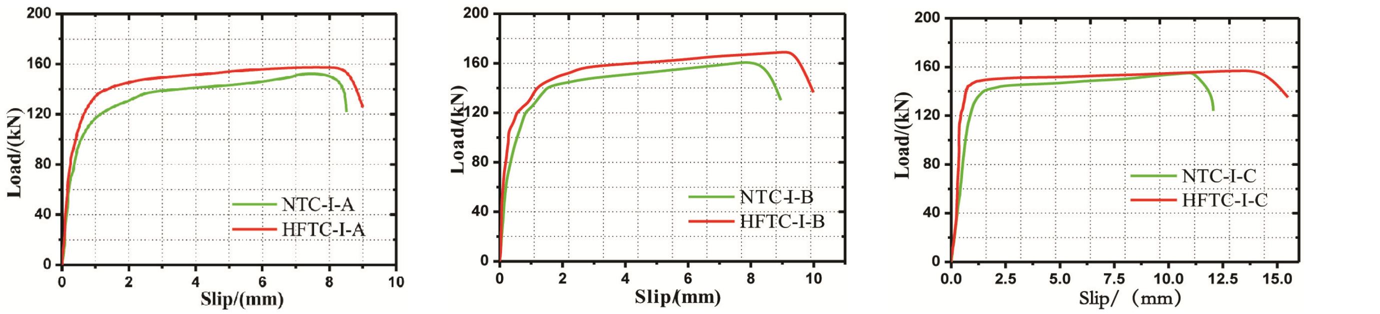

(a) Φ22-single stud (b) Φ22-double stud (c) Φ22-three stud

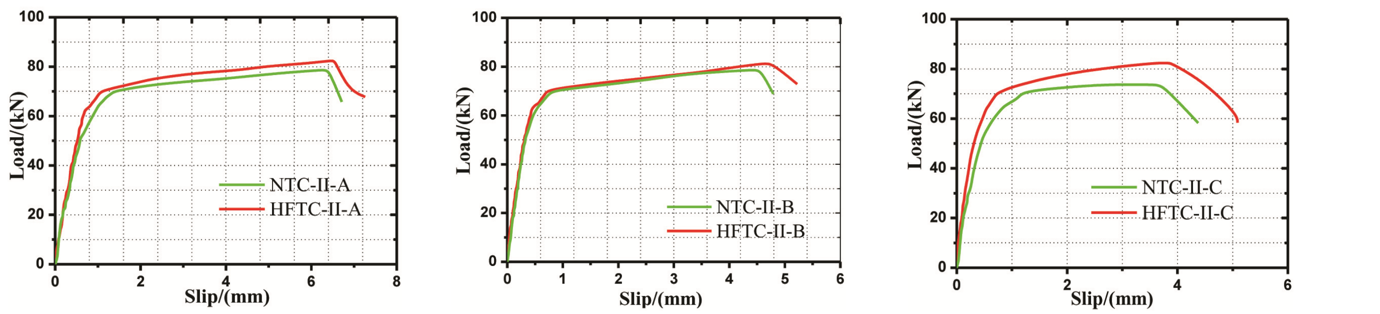

(d) Φ16-spacing 50 mm (e) Φ16-spacing 100 mm (f) Φ16-spacing 150 mm

Fig. 5 Comparison of load-slip curve for HFTC and NTC specimens

Table 7 Stiffness of a stud shear connector

Specimen		Xue *et al*. (2010) /(kN/mm)	Johnson (1994) /(kN/mm)	Kim *et al*. (2015) /(kN/mm)	Average stiffness /(kN/mm)
NTC-I	A	298	218	282	289
	B	303	225	288	
	C	309	235	296	
NTC-II	A	131	65	90	122
	B	146	85	124	
	C	165	113	151	
HFTC-III	A	418	381	396	367
	B	386	361	365	
	C	355	329	339	
HFTC-II	A	118	108	114	155
	B	185	165	171	
	C	186	169	181	
HFTC-III	A	133	118	128	156
	B	199	178	183	

developing further and enhanced the ductility of the stud connector.

The initial stiffness of stud shear connectors was assumed infinite according to the strength design concept. In the fact, they showed some initial slip in the early loading stage owing to surrounding concrete cracking and stud deforming. Kim *et al*. (2015) calculated the initial stiffness from the relative slip between 10% and 40% of the ultimate load. Xue *et al*. (2012) defined the stiffness of the connector as the secant slope at the slip of 0.2 mm, while Johnson (1994) defined as the secant stiffness at half shear connector ultimate load. The average stiffness of stud shear connectors was defined according to Kim *et al*. (2015) in this paper, as listed in Table 7. The average stiffness of NTC-I and NTC-II is 289 kN/mm and 122 kN/mm for single stud respectively, and HFTC-III specimens show the highest stiffness of 367 kN/mm. HFTC-IIand HFTC-III specimens have smaller stiffness (155 and 156 kN/mm. respectively) than HFTC-III. The stiffness of the shear connector calculated according to Xue *et al*. (2012) and Kim *et al*. (2015) was equivalence for the NTC specimens, and the stiffness calculated by Johnson's method was smallest. The stiffness of the shear connector calculated was almost equal according to Xue *et al*. (2012), Johnson (1994) and Kim *et al*. (2015) for the HFTC specimens. It showed that the stiffness of the NTC specimens declined faster at half shear connector ultimate load in comparison to the HFTC specimens.

The load-slip curves for the HFTC specimens had almost the same change trend with a varying ratio of space-to-stud numbers (Fig. 4). With increasing stud number, the slippage of the stud connector increased (Table 6), and the stiffness decreased (Table 7). The influence of the stud number on the shear bearing capacity was not obvious, and there is only a difference of 6% among the HFTC-I specimens (Table 6). While the stud spacing increased in the transverse direction, the stiffness of the stud connector increased slightly (Table 7), the slippage declined, the influence of the horizontal spacing on the shear bearing capacity was neglected, and there was a difference of only 5% among the HFTC-II specimens (Table 6). When the vertical spacing of the studs increased for the HFTC-III specimens, the shear bearing capacity, the stiffness and slippage declined slightly (Tables 6-7). Compared with NTC specimens, the bearing capacity of the HFTC specimens is little bigger (Table 6). This result is consistent with the findings of An and Cederwall (1996), who reported that the increase of maximum shear load of the shear connectors was about 34% when the cylinder compressive strength of the concrete increased from 30 to 81 N/mm^2 (45.1 Mpa for HFRC, 38.9 Mpa for NC as listed in Table 3). The slippage of the HFTC specimens is little bigger than that of the NTC specimens (Table 6). This may be attributed to the high ductility of the HFRC slabs. Table 7 also indicated that a stud embedded in the HFRC provides higher stiffness than that in the NC.

4. Evaluation of the push-out test results

4.1 Shear bearing capacity of HFRC push-out test

At present, equations to predict the ultimate resistances of shear connectors were developed based on push out test data for lightweight, normal weight, normal strength concrete and high-strength concrete, and equations to predict the ultimate resistance of shear connectors embedded in the HFRC are not available. Current design codes provide equations to compute ultimate resistance of a shear connector, mainly depending on the failure mode of the shear connections or concrete failure. The ultimate shear connector resistance for shear connector failure (P_{us}) provided by GB50017 (2003), ACI318-11 (2011), AISC (2011), AASHTO (2010) and PCI (2004) is computed by

Eq. (4).

$$P_{us} = A_s f_u \tag{4}$$

In the EN 1994-1-1 (2004) proposal, the shear connectors' resistance determined by a headed stud is suggested a reduction factor of 0.8 in Eq. (4) to computer the P_{us} (Eq. (5))

$$P_{us} = 0.8 A_s f_u \tag{5}$$

Where A_s is the cross-sectional area of the connector (mm^2), f_u is ultimate tensile strength of the stud (MPa).

For concrete failure, AISC (2011) and AASHTO (2010) recommend the same equation to determine the ultimate shear connector resistance (P_{uc}), which was originally developed by Ollgaard *et al*. (1971) (Eq. (6)).

$$P_{uc} = 0.5 A_s \sqrt{f_c' E_c} \tag{6}$$

The ultimate shear connector resistance for concrete failure (P_{uc}) provided by ACI318-11 (2011), PCI (2004), EN 1994-1-1 (2004), and GB50017 (2003) are presented in Eqs. (7)-(10), respectively

ACI: $$P_{uc} = k_{cp} 24\lambda \sqrt{f_c'}\ (h_{ef})^{1.5} \tag{7}$$

PCI: $$P_{uc} = 215\lambda \sqrt{f_c'}\ d^{1.5} (h_{ef})^{0.5} \tag{8}$$

EN 1994-1-1 (2004): $$P_{uc} = 0.29 \alpha d^2 \sqrt{f_{ck} E_{cm}} \tag{9}$$

GB50017: $$P_{uc} = 0.43 A_s \sqrt{f_c E_c} \tag{10}$$

Where k_{cp} is coefficient for pry-out strength (k_{cp} = 1 for h_{ef} < 2.5 in. and k_{cp} = 2 for h_{ef} > 2.5 in.); h_{ef} = effective embedment depth of headed stud shear connectors; d is the diameter of the shank of the stud (mm); λ is a modification factor reflecting the reduced mechanical properties of lightweight concrete (λ = 1 for normal weight concrete); f_{ck} is the characteristic value of concrete cylinder compressive strength (MPa); E_{cm} is the secant elastic modulus of concrete (GPa); and α is a coefficient defined as follows: $\alpha = 0.2(h/d + 1) \leq 1.0$; f'_c is the specified compression strength of the concrete (MPa), f_c is the cube compression strength of concrete (MPa), and E_c is the elastic modulus of concrete (GPa).

To the authors' knowledge, there has been no equation to determine the ultimate resistance of the stud shear connector embedded in HFRC. Eqs. (4)-(10) provided by the current design codes are based on test results of push-out specimens for lightweight, normal weight, and normal strength concrete, and they were used to compare against the experimentally obtained ultimate shear connector resistance form all specimens in this paper. Table 8 listed the test results and their comparison. The shear capacities from the Standards GB50017 2003, PCI 2004, ACI318-112011, AISC 2011, and AASHTO 2010 were, on average, 8% higher than the experimental values from the HFTC specimens and 9% higher than the value obtained from the NTC specimens for shear connector failure (P_{us}). The equation recommended by EN 1994-1-1 (2004) under-estimated, on average, 15% of the shear capacity of the HFRC slab headed studs for shear connector failure, and this difference was 12% for NTC specimens. It can be concluded that the code equations for predicting the ultimate resistance of the stud shear connectors for shear connector failure mode compare relatively well with the experimental results, with EN 1994-1-1 (2004) being more safer for HFTC specimens, however, the coefficient of variation was high (18.2% for HFTC specimens, 11.1% for NTC specimens) for EN 1994-1-1 (2004) analyzed.

The equations for predicting the ultimate shear connector resistance for concrete failure (P_{uc}) provided by AISC 2011 and AASHTO 2010, and GB50017 2003 were non-conservative compared to the experiment, with PCI 2004 and EN 1994-1-1 (2004) being more accurate (Table 8). On the other hand, ACI 318-112011 equation to predict the P_{uc} provides too conservative results for all specimens. The more conservative results obtained for ACI 318-112011 equation may be attributed to its assumption of concrete breakout failure, while the concrete breakout failure was not observed for all tested specimens in this study.

The design value of the ultimate shear connector resistance should be taken as a smaller value of the P_{us} and the P_{uc}. Table 8 indicates that ACI 318-11 2011 and PCI 2004 equations predicted a concrete failure for all tested specimens (since $P_{uc} < P_{us}$) while AISC 2011, AASHTO 2010, GB50017 2003, and EN 1994-1-1 (2004) equations predicted a shear connector failure (since $P_{us} < P_{uc}$). Strictly speaking, the experimental results indicated that the observed failure modes for all specimens were mixed failures (that included failures of the stud shear connectors and the localized crushing of concrete bellow the stud welded collar) in this study. But, none of the tested specimens failed by concrete breakout failure of the slabs. Therefore it can be concluded that the AISC2011, AASHTO 2010, and EN 1994-1-1 (2004) equations were more accurate than those provided by ACI 318-11 2011 and PCI 2004 in predicting the failure modes for the push-out specimens with the stud shear connectors embedded in the HFRC slabs.

The code equations to predict the ultimate shear connector resistance were developed for push-out specimens with a single failure mode (i.e., concrete failure or shear connector failure). But the fibers were incorporated into the NC, and the roughness, tensile and compression strength of the HFRC was higher than that of NC. It is difficult to consider the properties' improvement of HFRC for the code equations (Eqs. (4)-(10)) as observed in this study. Oehlers and Johnson (1987) proposed an equation to predict the ultimate shear connector resistance considering contributions of both shear connectors and concrete.

Oehlers and Johnson (1987) proposed one formula including contributions for both studs and concrete. The stud shear bearing capacity was determined by

$$\begin{gathered} P_{u\text{-}OJ} = K_{ch} A_s f_u (E_c / E_s)^{0.4} (f_c' / f_u)^{0.35} \\ K_{ch} = 4.7 - \frac{1.2}{\sqrt{N_{gr}}} \end{gathered} \tag{11}$$

Table 8 Comparison of test results and calculated values

Specimen	P_u /(kN)	P_u/P_{us} (shear connector failure) ACI, AISC, AASHTO, PCI, & GB50017 (Eq. (4))	EN 1994-1-1 (2004) (Eq. (5))	AASHTO & AISC (Eq. (6))	P_u/P_{uc} (concrete failure) ACI (Eq. (7))	PCI (Eq. (8))	EN 1994-1-1 (2004) (Eq. (9))	GB50017 (Eq. (10))	$P_u/P_{u\text{-}OJ}$ Oehlers and Johnson (Eq. (11))	$P_u/P_{u\text{-}MOJ}$ Empirical equation (Eq. (12))
HFTC-I-A	157.5	0.96	1.20	0.73	2.4	1.13	0.96	0.68	1.17	1.07
HFTC-I-B	169.6	1.04	1.30	0.78	2.58	1.21	1.03	0.73	1.24	1.05
HFTC-I-C	157.2	0.96	1.20	0.73	2.4	1.12	0.96	0.68	1.15	0.94
HFTC-II-A	82.5	0.91	1.14	0.72	2.02	1.12	0.95	0.67	1.18	1.00
HFTC-II-B	81.3	0.90	1.12	0.71	1.99	1.10	0.94	0.66	1.16	0.98
HFTC-II-C	82.5	0.91	1.14	0.72	2.02	1.12	0.95	0.67	1.18	1.00
HFTC-III-A	73.8	0.82	1.02	0.64	1.81	1.00	0.85	0.6	1.05	0.89
HFTC-III-B	78.8	0.87	1.09	0.69	1.93	1.07	0.91	0.64	1.12	0.95
Average	**110.4**	**0.92**	**1.15**	**0.72**	**2.1**	**1.11**	**0.94**	**0.67**	**1.16**	**0.985**
Coefficient of variation		**0.082**	**0.182**	**0.397**	**0.598**	**0.133**	**0.073**	**0.507**	**0.173**	**0.062**
NTC-I-A	152.5	0.93	1.17	0.76	2.5	1.17	0.95	0.72	1.15	
NTC-I-B	162.5	0.99	1.24	0.80	2.66	1.25	1.01	0.77	1.23	
NTC-I-C	155.5	0.95	1.19	0.77	2.55	1.20	0.97	0.74	1.15	
NTC-II-A	78.8	0.87	1.09	0.74	2.08	1.15	0.92	0.71	1.10	
NTC-II-B	78.8	0.87	1.09	0.74	2.08	1.15	0.92	0.71	1.10	
NTC-II-C	73.8	0.82	1.02	0.69	1.95	1.08	0.86	0.66	1.03	
Average	**117**	**0.91**	**1.12**	**0.75**	**2.30**	**1.17**	**0.94**	**0.72**	**1.14**	
Coefficient of variation		**0.082**	**0.111**	**0.285**	**0.541**	**0.151**	**0.075**	**0.339**	**0.148**	

*Note: P_u = experimentally obtained ultimate resistance of a shear connector; P_{us} = ultimate shear connector resistance for shear connector failure; P_{uc} = ultimate shearconnector resistance for concrete failure; $P_{u\text{–}OJ}$ = ultimate shear connector resistance determined from Oehlers and Johnson's equation; $P_{u\text{–}MOJ}$ = shearresistance of a shear connector modified from Oehlers and Johnson's equation

where A_s is the cross-sectional area of the connector (mm^2), f'_c is the specified compression strength of concrete (MPa), f_u is ultimate tensile strength of the stud (MPa), N_{gr} is the number of shear connectors that can be assumed to fail as a group, E_c is the elastic modulus of concrete (GPa), and E_s is the elastic modulus of steel (GPa).

The $P_u/P_{u\text{-}OJ}$ ratio was computed as shown in Table. 8. Oehlers and Johnson (1987) for predicting the ultimate shear connector resistance underestimated the experimental results of HFTC specimens. This may be attributed not to consider the properties' improvement of HFRC used for HFTC specimens in this study. The average E_c and f'_c obtained experimentally for the HFRC are higher than that of NC (Table 3). Therefore the variables for the E_c and f'_c in Eq. (11) should be replaced by E_{fc} and f'_{fc} to compute the ultimate resistance of the shear connector embedded in the HFRC slabs. Oehlers and Johnson (1987) suggested that the material bounds for concrete of $10 < E_c < 33$ kN/mm^2 and $24 < f'_c < 81$ N/mm^2 should be used in Eq. (11). The average E_{fc} and f'_{fc} obtained experimentally for the HFRC are no more than the maximum material bounds of concrete suggested by Oehlers and Johnson (1987). So the powers for the E_{fc}/E_s (0.4) and f'_{fc}/f_u (0.35) ratios keep invariable in Eq. (12). The HFRC slab was used for push out tests in this study and it had relatively high roughness, tensile and compression strength, and bearing strength as compared to the conventional concrete slab. An and Cederwall (1996) also reported that the maximum shear load of the shear connectors increased when the cylinder compressive strength of the concrete increased from 30 to 81 N/mm^2. Chi *et al*. (2014b) gave an equation for calculating the HFRC uniaxial compressive strength in Eq. (1). New parameters λ_{sf} and λ_{pf} were thus introduced in Eq. (12) to account further for the effect of the SF and PF to the ultimate shear connector resistance. The coefficients of the λ_{sf} and λ_{pf} fetched 0.206 and 0.388 respectively according to Eq. (1).

$$P_{u-MOJ} = K_{ch}(1+0.206\lambda_{sf}+0.388\lambda_{pf})A_s f_u (E_{fc}/E_s)^{0.4}(f'_{fc}/f_u)^{0.35} \quad (12)$$

Where A_s is the cross-sectional area of the connector (mm^2); f'_{fc} is the specified compression strength of HFRC (MPa), respectively; f_u is ultimate tensile strength of the stud (MPa); E_{fc} is the elastic modulus of HFRC (GPa); E_s is the elastic modulus of steel (GPa).

$P_{u\text{–}MOJ}$ is the ultimate shear connector resistance modified from Oehlers and Johnson (1987), showed moreaccurate results as compared to code equations. The coefficient of variation (CV) for the computed $P_{u\text{-}MOJ}$ using Eq. (12) is lowest as listed in Table 8. These results indicate that the proposed empirical equation can be potentially used to predict the ultimate shear connector resistance for HFTC specimens. However, the authors suggest that more push-out test data of the steel-HFRC composite girder system are needed to verify the applicability of the proposed empirical equations.

4.2 Load-slip relationship for HFTC specimens

The load-slip curve can display the static behavior of stud shear connectors. For example, the ductility of the stud connectors can be explained by the slippage of the load-slip curve between the concrete slab and steel beam. The load-slip curves were mainly obtained using push-out tests, curve fitting was performed to find fitting parameters for all tested specimens, and then the empirical equation of the load–slip behavior was available. For comparison purposes, the P/P_u ratio versus slip relationships for reloading/continuous loading condition obtained from empirical equations proposed by Buttry (1965) (Eq. (13)), Ollgaard *et al*. (1971) (Eq. (14)), and An and Cederwall (1996) (Eq. (15)) were also included in Fig. 7 in the study. Eqs. (13)-(15) were used for push-out tests of steel-concrete composite girders with studs embedded in normal strength concrete (Eqs. (13)-(14)) and high strength concrete (Eq. (15)).

$$P/P_u = 80s/(1+80s) \tag{13}$$

$$P/P_u = (1-e^{-18s})^{2/5} \tag{14}$$

$$P/P_u = \frac{4.44(s-0.031)}{1+4.24(s-0.031)} \tag{15}$$

Where P is the applied load of the stud (kN), P_u is the measured maximum load per stud (kN), and s is the slippage, s is in inch for Eqs. (13)-(14) and in millimeter for Eq. (15).

Non-linear regressions of the experimental load–slip curves ofthe five series specimens were performed (Fig. 7). Eq. (14), suggested by Ollgaard *et al*. (1971) for headed stud connectors associated with solid slabs, was used for the regression, and the effect of SF and PF was considered (Eq. (16)).

$$P/P_u = (1-e^{-(a+b\lambda_{sf}+c\lambda_{pf})s})^{\beta} \tag{16}$$

The characteristic slip capacity is compose of the shear deformation of stud and the flexural deformation of stud as a result of the local concrete crushing and cracking below the stud. So the specified compression strength of concrete has significant influence on the slippage. Chi *et al*. (2014b) gave an equation for calculating the HFRC uniaxial compressive strength in Eq. (1). Since this study only conducted a combination of SF (1%) and PF (0.15%). In order to facilitate the regression, the b and c fetched 0.206 and 0.388 respectively according to Eq. (1). Values of a = 2.11 and β = 0.86 mm^{-1} were obtained from the regression for the HFTC specimens (Eq. (17)), and a = 1.7, b = 0, c = 0 and β = 0.9 mm^{-1} were obtained for the NTC specimens (Eq. (18)). The new expressions of the load-slip relationship were given by

$$P/P_u = (1-e^{-(2.11+0.206\lambda_{sf}+0.388\lambda_{pf})s})^{0.86} \tag{17}$$

$$P/P_u = (1-e^{-1.7s})^{0.9} \tag{18}$$

Eqs. (13)-(14) underestimated the relationships between the P/P_u ratio and slip for all the specimens (Fig. 6). This may be attributed to the smaller slip per P/P_u ratio of the tested specimens as compared to the slip per P/P_u ratio determined by the empirical equations. The values estimated by Eq. (15) agreed well with the test results of HRTC specimens (Fig. 6(b)). The cause is the empirical equations (Eqs. (13)-(14)) were developed for steel–conventional concrete composite girder system, where studs were embedded in normal strength concrete, resulting in a slightly larger slip per P/P_u ratio. While Eq. (15) was applied for the shear connectors embedded in high strength concrete, resulting in a slightly smaller slip per P/P_u ratio. On the other hand, the shear connectors in this study were embedded in HFRC, and the properties' improvement of concrete may also result in a slightly smaller slip per P/P_u ratio. The P/P_u ratio versus slip relationship obtained from Eqs. (15) and (18) showed a higher stiffness, while those obtained from Eqs. (13)-(14) showed slightly lower

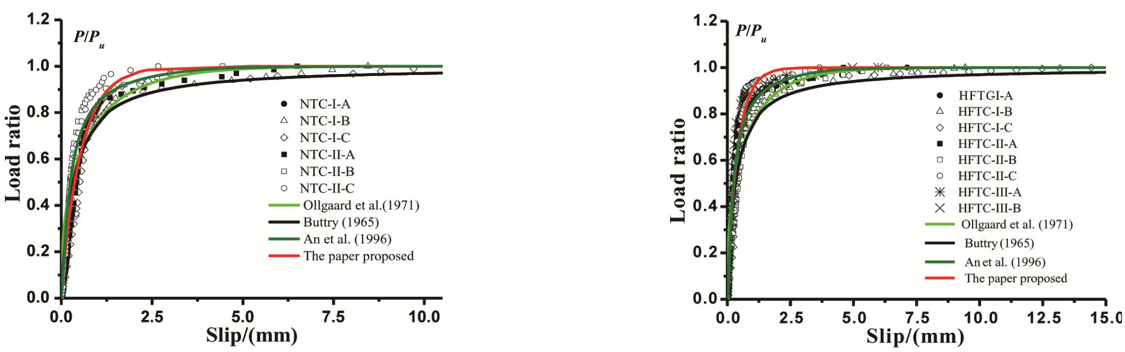

(a) NTC specimens (b) HFTC specimens

Fig. 6 Comparison of test results, empirical equations and regression curve stiffnesses. Fig. 6(b) indicates that the P/P_u ratio versus slip relationships obtained from the empirical equations (Eq. (18)) for the HFTC specimens showed a better correlation with the experimental result. This result implies that the empirical equations may predict the P/P_u ratio versus slip relationship of shear connectors embedded in the HFRC with higher accuracy. Therefore, the empirical equation of the load-slip curves obtained in this paper may provide certain references for the design of steel-HFR composite structures.

5. Conclusions

This study investigated experimentally the composite action between the HFRC deck and steel beam. 14 push-out tests (five batches) were performed in HFRC and NC. Parameters in the specimens were the type of decks, number of studs, and diameter of studs. The load-slip curves and equations to predict the ultimate resistance of the shear connectors in HFRC slabswere discussed. Push-outtest results of the deck-to-steel beam connections were summarized as follows:

- The stud connector in HFRC slab has a higher stiffness, ductility and slightly larger shear capacity than the stud connector in NC. Increasing the transverse spacing and the number of studs had a neglected effect on shear bearing capacity per stud, and then had an obvious influence on the slip and stiffness. The stiffness, shear bearing capacity, and slippage declined slightly when the vertical spacing of the studs increased.
- An empirical equation to predict the ultimate resistance of the stud shear connectors embedded in the HFRC slabs was proposed. The proposed empirical equation was established for shear connections of the steel-HFRC composite girder system taking into account the effects of SF and PF. The ultimate resistance of the stud shear connectors predicted by the empirical equation compares relatively well with that obtained experimentally. Although the proposed empirical equation can be potentially used to evaluate the ultimate resistance of the steel-HFRC shear connections, the authors suggest that more push-out test data and analysis are needed to verify its applicability.
- Curve fitting was performed to find fitting parameters for all push-out tested specimens. Idealized load–slip models and equations to predict the load versus slip relationship for the specimens were proposed. A proposed exponential equation can be effectively used to predict the load–slip behavior for HFTC specimens.

The stud shear connector embedded in HFRC slab has a different mechanical behavior from that of NC, which provides an alternative method to decrease the cracks of the slabs deck in composite bridge. All the findings at present study may provide reference for application of the stud shear connector embedded in HFRC. The next steps of the present investigation will consider more push-out tests and full scale tests of composite beams using HFRC slabs deck. These further studies will help to bring HFRC slab deck into practice use.

Acknowledgments

This work was financially supported by Cyrus Tang Center for Sensor Materials and Applications, Zhejiang University, and the 2011 Science and Technology Project of the Hangzhou Construction Committee.

References

AASHTO (2010), Bridge design specifications; (5th Ed.), AASHTO LRFD, Washington, DC, USA.

ACI 318 (2011), Building code requirements for structural concrete and commentary; Farmington Hills, MI, USA.

ACI-Committee-544 (2009 Reapproved), Report on Fiber Reinforced Concrete; ACI 544.1R-96.

AISC (2011), Specification for structural steel buildings; American Institute of Steel Construction (AISC), Chicago, IL, USA.

An, L. and Cederwall, K. (1996), "Push-out tests on studs in high strength and normal strength concrete", *J. Constr. Steel Res.*, **36**(1), 15-29.

Buttry, K.E. (1965), "Behavior of stud shear connectors in lightweight and normal-weight concrete", University of Missouri-Columbia, MO, USA.

Caggiano, A., Gambarelli, S., Martinelli, E., Nisticò, N. and Pepe, M. (2016), "Experimental characterization of the post-cracking response in hybrid steel/polypropylene fiber-reinforced concrete", *J. Constr. Build. Mater.*, **125**(30), 1035-1043.

CECS (2004), Fiber concrete structure technical regulation; China Planning Press, China. [In Chinese]

Chi, Y. (2012), "Plasticity theory based constitutive modeling of hybridfibre reinforced concrete", Ph.D. Thesis; University of Nottingham, Nottingham, UK.

Chi, Y., Xu, L.H. and Yu, H.S. (2014a), "Plasticity model for hybrid fiber reinforced concrete", *J. Eng. Mech.*, **140**(2), 393-405.

Chi, Y., Xu, L.H. and Zhang, Y. (2014b), "Experimental study on hybrid fiber-reinforced concrete subjected to uniaxial compression", *J. Mater. Civil Eng.*, **26**(2), 211-218.

Demir, A. (2015), "Prediction of hybrid fibre-added concrete strength using artificial neural networks", *Comput. Concrete, Int. J.*, **15**(4), 503-514.

EN 1994-1-1 (2004), Eurocode 4: Design of composite steel and concrete structures – Part 1-1: General rules and rules; European Standard.

GB50017 (2003), Code for design of steel structures; China Planning Press, China. [In Chinese]

Han, Q.H., Xu, J., Xing, Y. and Li, Z.L. (2015), "Static push-out test on steel and recycled tire rubber-filled concrete composite beams", *Steel Compos. Struct., Int. J.*, **19**(4), 843-860.

Huang, C.K. (2004), "Structure of fiber reinforced concrete", China Machine Press, Beijing, China. [In Chinese]

Johnson, R.P. (1994), *Composite Structures of Steel and Concrete*, (2nd Ed.), Volume 1, Blackwell Scientific Publications, Ltd., Oxford, UK.

Kim, J.S., Kwark, J., Joh, C., Yoo, S.W. and Lee, K.C. (2015), "Headed stud shear connector for thin ultrahigh-performance concrete bridge deck", *J. Constr. Steel Res.*, **108**, 23-30.

Kim, N.W., Lee, H.H. and Kim, C.H. (2016), "Fracture behavior of hybrid fiber reinforced concrete according to the evaluation of crack resistance and thermal", *Comput*. *Concrete*, **18**(5), 685-696.

Lam, D. and El-Lobody, E. (2005), "Behavior of headed stud shear connectors in composite beam", *J. Struct*. *Eng*., **131**(1), 96-107.

Mara, V., Haghani, R. and Harryson, P. (2014), "Bridge decks of fibre reinforced polymer (FRP): A sustainable solution", *J. Constr*. *Build*. *Mater*., **50**, 190-199.

Nguyen, H., Mutsuyoshi, H. and Zatar, W. (2014), "Push-out tests for shear connections between UHPFRC slabs and FRP girder", *Compos. Struct*., **118**, 528-547.

Oehlers, D.J. and Johnson, R.P. (1987), "The strength of stud shear connections in composite beams", *Struct*. *Eng*., **65**(2), 44-48.

Ollgaard, H.G., Slutter, R.G. and Fisher, J.D. (1971), "Shear strength of stud Connectors in lightweight and normal-weight concrete", *AISC Eng*. *J*., **8**(2), 55-64.

PCI (2004), Precast/prestressed concrete institute design handbook: Precast and prestressed concrete; (6th Ed.), Chicago, IL, USA.

Prisco, M.D., Plizzari, G. and Vandewalle, L. (2009), "Fibre reinforced concrete: New design perspectives", *Mater*. *Struct*., **42**(9), 1261-1281.

Qian, C.X. and Stroeven, P. (2000), "Development of hybrid polypropylene-steelfibre-reinforced concrete", *Cement Concrete Res*., **30**(1), 63-69.

Tuan, B.L.A., Tesfamariam, M.G., Hwang, C.L., Chen, C.T., Chen, Y.Y. and Lin, K.L. (2014), "Effect of fiber type and content on properties of high-strength fiber reinforced self-consolidating concrete", *Comput*. *Concrete*, *Int*. *J*., **14**(3), 299-313.

Xue, D., Liu, Y., Yu, Z. and He, J. (2012), "Static behavior of multi-stud shear connectors for steel-concrete composite bridge", *J. Constr*. *Steel Res*., **74**, 1-7.

Zhang, Y. (2010), "Study on uniaxial compressive constitutive relationship and uniaxial tensile behavior of steel-polypropylene hybrid fiber reinforced concrete", Ph.D. Thesis; Wuhan University, Wuhan, China. [In Chinese]

DL